SCIENCE and ART: A Future for Stone

Proceedings of the 13th International Congress on the Deterioration and Conservation of Stone – Volume I

SC16

Edited by
John Hughes & Torsten Howind

SCIENCE AND ART: A FUTURE FOR STONE

PROCEEDINGS OF THE 13TH INTERNATIONAL CONGRESS ON THE DETERIORATION AND CONSERVATION OF STONE

6th to 10th September 2016, Paisley, Scotland

VOLUME I

Edited by
John J. Hughes and Torsten Howind

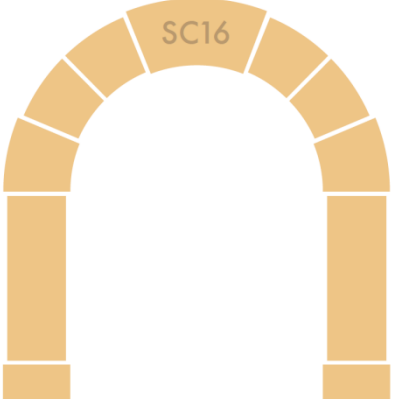

UNIVERSITY OF THE WEST of SCOTLAND
UWS

INTRINSIC PARAMETERS CONDITIONING THE FORMATION OF MN-RICH PATINAS ON LUNEVILLE SANDSTONES

L. Gatuingt[1*], S. Rossano[2], J.-D. Mertz[3], B. Lanson[4] and O. Rozenbaum[5]

Abstract

After a fire in 2003 and thus, after being submitted to a large quantity of water, part of the sandstones of the Luneville castle (XVIIIth century, France) developed a dark Mn-rich patina within a few weeks. This phenomenon is also observed on sandstones only subjected to rainwater but with a formation time of the order of several years. This project aims to better understand the formation mechanisms of dark Mn-patinas, especially in the Luneville castle case, focussing on the characteristics of the sandstones. In order to investigate intrinsic factors conditioning the formation of a patina, two pairs of representative stones (patinated/unpatinated) have been sampled on site, in the burnt and unburnt zones respectively. Macroscopic and microscopic observations and Inductively Coupled Plasma-Optical Emission Spectrometry (ICP-OES) were employed to obtain global, visual and chemical information on the bulk material. Optical and electronic microscopies, coupled with Energy-Dispersive X-ray Spectroscopy (EDS) establish a correlation between the visual aspect of an area and its Mn-content. Quantitative chemical data on selected regions of interest were obtained by Particle-Induced X-ray Emission (PIXE) method, to derive the Mn-chemical environment. Mercury intrusion porosimetry, capillary imbibition and permeability measurements have also been made to evaluate the impact of the rock transfer properties on the patina's development. Petrophysical properties of the sandstones facilitate water transport, but no significant differences have been underlined between patinated and unpatinated blocks. However, the sandstones which developed a patina contain a greater Mn-quantity than the others. Moreover, the chemical associations in Mn-rich areas are not the same, suggesting different original Mn-bearing phases.

Keywords: sandstone, manganese, patina

[1] L. Gatuingt*
Laboratoire de Recherche des Monuments Historiques CRC-LRMH-USR3224, Laboratoire Géomatériaux et Environnement, Université Paris-Est, France
laure.gatuingt@culture.gouv.fr

[2] S. Rossano
Laboratoire Géomatériaux et Environnement, Université Paris-Est, France

[3] J.-D. Mertz
Laboratoire de Recherche des Monuments Historiques CRC-LRMH-USR3224, France

[4] B. Lanson
ISTerre, CNRS, Université Grenoble Alpes, F-38041, France

[5] O. Rozenbaum
ISTO, Université d'Orléans CNRS BRGM, UMR7327, France

*corresponding author

1. Introduction

The Luneville castle, located in the North-East part of France, was built during the XVIIIth century with local Buntsandstein sandstones of various colourations. In January 2003, a violent fire affected the castle submitting building sandstones to an increase of their surface temperature and to an important volume of water (~21 m^3/min during ~10 hours). Several weeks later, black-brown patinas started developing on burnt parts of the castle (~8 % of the 1500 m² of exposed sandstones). Areas that have not been submitted to the accidental fire, may also present patinas formed over a long time range in natural environments as described for other buildings (Thomachot and Jeannette, 2004; Mertz, 2010). While it has been shown that the dark patinas contain iron oxides and sometimes manganese (oxihydr)oxides (Nord and Ericsson, 1993; Thomachot and Jeannette, 2004), the precise mineralogical compositions of these dark layers as well as their formation mechanisms remain to be determined. Besides, for given environmental solicitations (unburnt or burnt and watered area), and same period of implementation on the monument, the formation of dark stains is not systematic.

The main objective of this work is to characterise sandstone samples in order to identify intrinsic factors related to the development of the different patinas (short-time and long-time set-up). Chemical compositions of the rocks as well as storage and transfer properties of water in the sandstones have been measured, combining analytical techniques. Total rock chemical analyses have been obtained by Inductively Coupled Plasma-Optical Emission Spectrometry (ICP-OES). Optical microscopy (OM) and scanning electron microscopy coupled with Energy Dispersive Spectrosocopy (SEM-EDS) have been used to describe the samples and localize regions of specific interest which composition have been obtained by the Particle-Induced X-ray Emission (PIXE) method. The porous networks have been characterised by mercury intrusion porosimetry (MIP), capillary and permeability measurements.

2. Materials and methods

2.1. Materials

Buntsandstein sandstones (lower Triassic, ~250 My) are related with a deltaïc sedimentation environment (Perriaux, 1961 ; Colas 2011), and are mainly composed of quartz, K-feldspars, lithic fragments, micas, clay minerals and various oxides (Beyer, 1983; Soyk, 2015). The stone colouration is white for low Fe-content. For high Fe-content, colouration is yellow or red depending on the main Fe-bearing phase (goethite and hematite, respectively – Soyk, 2015). Most of the building stones of the castle are yellow.

Macroscopically similar (texture and grain size) pairs of yellow stones (patinated/unpatinated) have been sampled on site, in the burnt and highly watered (L2/L5) and unburnt (L1/L4) areas. The sampled volume is about 20×30×10 cm^3 for each block. Polished and unpolished sections, powders and cores had been prepared from the blocks. Information about the different preparations in terms of size, number of samples and performed analytical techniques are listed in table 1.

Tab. 1: Sample preparation and associated analytical techniques. N is the quantity per block.

Sample preparation	N	Analytical techniques
Polished section *(~15×15 mm²)*	1	OM, SEM-EDS
Unpolished section *(~15×15 mm²)*	1	OM, PIXE
Powder *(~2-3 g)*	1	ICP-OES
Core *(d=13 mm, h=9 mm)*	9	Mercury porosimetry
Core *(d=30 mm, h=60 mm)*	6 (4 for L1)	Capillarity, Permeability

2.2. Methods

OM pictures were obtained with a Keyence VHX-5000 microscope, with magnification ×20 or ×100. SEM-EDS observations were performed in backscattered electron mode, using a JEOL JSM 5600 LV SEM equipped with a tungsten filament operating at an accelerating voltage of 20 kV and using a low vacuum pressure (17 Pa) to avoid sample coating.

Bulk chemical compositions were determined from digested samples by ICP-OES at the Geochemical and Petrographic Research Center (CRPG, Nancy, F) following the procedure described in Carignan *et al.* (2001). PIXE analyses were performed on unpolished sections at the AGLAE facility using a proton energy of 3 MeV, and a 20 µm beam size. The detection system is detailed in Pichon *et al.* (2014).

The porous network of the four bulk samples was investigated by MIP using an Autopore IV Micrometrics® equipment. The applied pressures ranged 0.00226-206 MPa, corresponding to pore size radii of 270 µm and 0.003 µm, respectively. Three zones were selected for each block, and three measurements were made and averaged for each zone. Capillary imbibition measurements were conducted following the European standard procedure EN 1925. Cores were cut parallel to the bedding plans and their bases immersed in 3 mm of water. The kinetic coefficients of weight gain (A) and fringe's migration (B) were derived from Washburn equations. The average of the A and B coefficients have been calculated. Permeability values were acquired with a steady-state minipermeameter coupled with the software CYDAR™ (Cydarex Company, F). This is a non-destructive technique, which characterises the permeability until 21 mm depth in the sample. Air permeability measurements were averaged. For MIP, capillary and permeability measurements, error bars are equal to ± the standard deviation calculated for each analyzed zone.

3. Results and discussion

3.1. Visual description of the samples

Visual inspection of the four sandstone thin sections indicates great colour variability in patinated samples (L1 and L2 – Fig. 1). Yellow, orange and white stripes are observed in L1 parallel to the bedding and perpendicular to the exposed surface. Black dots, ~500 µm in diameter, are also distributed over the entire bulk. The coloured bands in L2 type are mostly brown and are combined with a series of different compaction zones. Consistent with the literature (Colas, 2011; Soyk, 2015) brown bands are likely related to Fe-oxihydroxides mixed with clay minerals. Non-patinated L4 and L5 are more homogeneous

than L1 and L2 and present uniform color and texture. However, small (~1 mm) over compacted zones and a mica-rich layer (~3 cm) are encountered in L4 and L5, respectively. The darker area observed on L5 (top left of the section – Fig. 1) is part of the mica-rich layer. For all samples, quartz grain size ranges 100-300 µm in diameter. The patina developed on L1 is ~350 µm thick while that on L2 is ~50 µm thick.

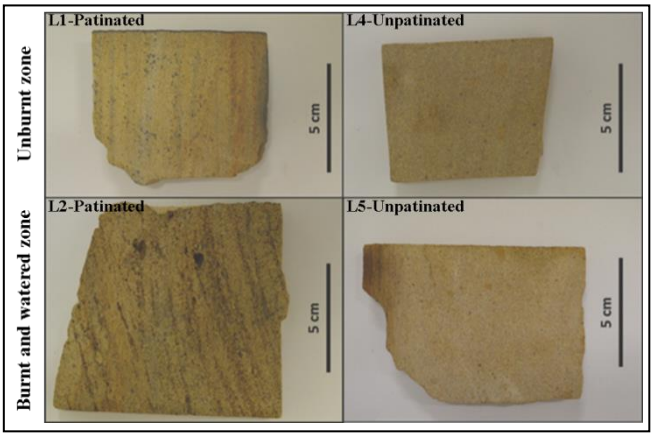

Fig. 1: Sample sections perpendicular to the bedding and to the surface. The exposed surfaces are positioned upward.

3.2. Storage and transfer properties

In order to obtain information on the properties of the porous networks and their variability in relation with texture, colour and compactness, porosity, capillary imbibition and permeability measurements have been performed for three areas of each block. The studied regions were chosen sufficiently far from the exposed surface, to ensure that the measurements are characteristic of the bulk sandstone. Core sizes for porosity measurements (13 mm in diameter) were chosen as small as possible to allow exploring millimetric heterogeneities in L1 and L4. By contrast, core size used for imbibition and permeability measurements (30 mm in diameter) is much greater than the size and the pattern of the heterogeneities. Measurements are reported in the Tab. 2 for the three zones.

MIP and capillary curves (not shown) are representative of unimodal pore size distributions and well-connected porous network. With total porosity values ranging from 18.5% to 26.1%, investigated samples rank among the most porous Buntsandstein sandstones (5%-25% - Thomachot and Jeannette, 2004; Colas, 2011). Permeability values from Luneville stones (87 to 880 mD) are typical for highly permeable quartzic sandstones (from 0.1 mD for not permeable to 1D for very permeable) (Gueguen and Palciaukas, 1992; Géraud, 2000). For all samples, capillary coefficients B lead to saturation times of a few hours for 60 mm sample length (2h56 for L1, 2h02 for L4, 1h00-1h34 for L2, and 1h09-2h38 for L5). Over 10 hours of continuous water flow such as long rainy episodes or during the 2003 fire extinction, at least 11 cm of rock may be invaded by water (considering the smallest B coefficient: 3.5 $cm \cdot h^{-1/2}$). Therefore, even if the cores were taken as far as possible from the surface, they may have been modified by the interaction with water and may not be representative of original sandstones.

*Tab. 2: MIP data (N_{Hg}=porosity), capillary (A and B) and permeability (K) coefficients. Grey lines correspond to patinated samples. UB (resp. B) corresponds to unburnt (resp. burnt) area. *****A, B and K values for L2 and L5 represent the average of measurements performed on 2 cores sampled in 3 different zones. A, B and K values for L1 (resp. L4) represent the average of measurements performed on 4 cores (resp. 6) sampled throughout the volume.*

	Sample	Zone	N_{Hg} (%)	A* ($g \cdot cm^{-2} \cdot h^{-1/2}$)	B* ($cm \cdot h^{-1/2}$)	K* (mD)
UB	L1	Orange	21.7 ±0.8	0.290 ±0.046	3.5 ±0.2	150 ±65
		white-yellow	21.6 ±0.3			
		Yellow	21.3 ±0.2			
	L4	White	21.6 ±0.9	0.388 ±0.019	4.2 ±0.2	118 ±41
		pale yellow	23.1 ±0.2			
		yellow	24.1 ±0.5			
B	L2	lightly uncompacted	23.9 ±0.1	0.433 ±0.001	4.8 ±0.2	759 ±34
		brown and uncompacted	26.1 ±1.7	0.549 ±0.028	5.3 ±0.4	880 ±245
		clearer	24.8 ±0.6	0.521 ±0.083	6.0 ±0.5	473 ±76
	L5	yellow	25.2 ±0.2	0.465 ±0.001	5.3 ±0.0	859 ±12
		yellow	24.8 ±0.2	0.490 ±0.041	5.6 ±0.2	632 ±1
		mica-rich layer	18.5 ±0.4	0.276 ±0.002	3.7 ±0.1	87 ±3

L1 shows important colour variability but the different coloured zones have similar porosity values. By contrast, for L4, porosity values are lower in the millimetric white over-compacted areas than in the yellow areas. In the L2 sample, the variability of all measured parameters from one zone to the other suggests a high heterogeneity. In L5, the two yellow areas studied have similar characteristics, whereas the mica-rich layer presents poorer storage and transfer properties. The unburnt blocks are more homogeneous than the burnt ones. Burnt blocks (L2 and L5) are more porous, more permeable, and have higher capillary properties than their unburnt counterparts. These characteristics are possibly related to the original block variability as the values are systematically consistent with those of Buntsandstein sandstones. But it could also be assumed that the amount of water used to drown the fire (~12720 m^3 i.e. ~2 l per block) was sufficient to saturate the porous network (1.1 l and 1.6 l for 18.5% and 26.1% porosity, respectively) thus inducing dissolution of mineral phases and porosity increase. Comparison of patinated samples (L1 and L2) with non-patinated samples (L4 and L5) does not lead to clear conclusions. L4 has slightly higher porous and capillary properties than L1, the two blocks having similar permeability. Except for the mica-rich zone in L5, which represents only a small part of its volume, L2 and L5 have similar macroscopic properties.

3.3. Chemical composition of the bulks and Mn content

Elemental bulk-rock analyses are given in Tab. 3. As for the other measurements, the powders have been produced from sandstone sampled as far as possible from the surface, to avoid its contribution. The concentrations of major elements are similar for all samples and lie in range known for Buntsandstein sandstones with high concentrations of oxides (Fe, Mn, Ti, P – Beyer, 1983; Thomachot et Jeannette, 2004; Colas, 2011). L2 is significantly enriched in Fe, which is consistent with the presence of numerous brown bands. The patinated blocks are also richer in Mn than the other ones (L1 is the richest and [Mn] is 10× larger in L2 than in L5).

Tab. 3: Sulphur content, ICP average chemical composition (oxide wt %) and loss of ignition (LOI) at 1000°C (in %) of the four bulks. Grey lines correspond to patinated samples. UB (resp. B) corresponds to unburnt (resp. burnt) area. Uncertainties are <20% for S, <15% for Ca, Na, and P, <10% for Mn, Mg, and Ti, <5% for K and LOI, <2% for Fe, <1% for Si, Al

Sample	SiO_2	Al_2O_3	Fe_2O_3	MnO	MgO	CaO	Na_2O	K_2O	TiO_2	P_2O_5	SO_3	LOI	Total
UB-L1	83.33	7.32	1.33	0.24	0.23	0.14	0.17	3.47	0.56	0.11	0.13	2.21	99.24
UB-L4	83.42	7.58	1.82	0.06	0.20	0.14	0.12	4.01	0.38	0.07	0.35	2.26	100.41
B-L2	81.56	7.02	3.64	0.10	0.14	0.16	0.14	4.36	0.23	0.12	0.08	1.80	99.35
B-L5	85.29	7.66	0.70	0.01	0.19	0.15	0.15	4.25	0.49	0.12	0.08	1.58	100.67

3.4. Mn-bearing phases in the bulk sandstones

Representative OM and SEM-EDS observations of the Mn-rich zones of L1 and L2 polished sections are shown in Fig. 2. Mn-rich zones in L5 and most Mn-rich zones in L4 are similar to those in L2. L4 presents a few zones similar to L1. Most Mn-rich zones in L1 appear as black dots distributed in the sandstone volume. In L2, Mn is mostly concentrated in very large stains (~500 μm) with red-brown and dark-brown colours. The Mn-rich areas are clearly more abundant in the patinated blocks. PIXE analyses were conducted on a Mn-rich area for each block (Tab. 4). For better clarity, only elements showing significant differences (i. e. Mn, Fe, Ba) are reported in the table. Mn concentrations in patinated samples (L1 and L2) are significantly higher than in their non-patinated counterparts (L4 and L5, respectively). Mn concentration is the highest in the L1 sample (between ×14 and ×54 as compared to Mn-rich areas in the other sandstones). By contrast with L2, L4 and L5, Mn-rich stains in L1 are characterised by a high Ba-content suggesting either the occurrence of Mn-Ba oxides, such as romanechite, hollandite, or todorokite, or the coexistence of Ba- and Mn-bearing phases. The absence of Ba in L4 black spots suggests the sole presence of Mn-bearing phases. No indication about the possible similarity between the phases can be deduced from chemical analyses. In L2, as in L5, Mn is less abundant as compared to unburnt sandstones, and is always associated with iron, which prevails over these areas. X-ray diffraction analyses (not shown) and morphological observations allowed identifying goethite as the main Fe-bearing mineral. It is known that Mn can be mixed with goethite, mainly as phyllomanganate (Manceau *et al.*, 2000), we can thus suspect such phases.

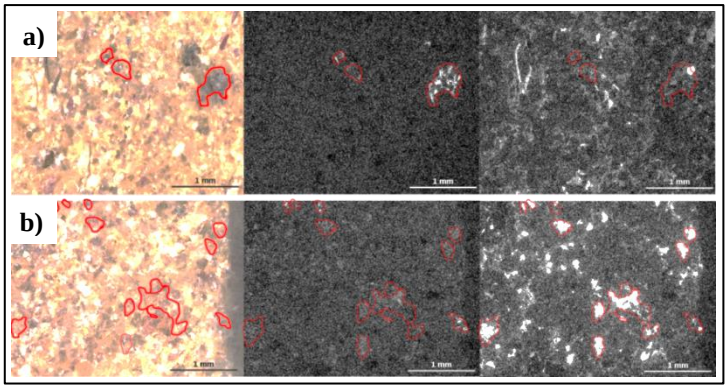

Fig. 2: Mn-bearing phases, circled in red, (a) in L1 and (b) in L2. Views on polished sections with, from left to right, optical microscopy, Mn and Fe maps obtained with EDS.

Tab. 4: PIXE analyses (oxide weight %) of Mn, Fe and Ba contained in Mn-rich areas (surfaces in µm²). Grey lines correspond to patinated samples.

Sample	Analysed surface	Fe_2O_3	MnO	BaO
L1	~500×300	3.16 ± 0.05	12.48 ± 0.06	11.91 ± 1.28
L4 *(L1-like)*	~200×200	2.37 ± 0.02	0.89 ± 0.01	0.00 ± 0.00
L2	~500×300	53.98 ± 0.51	0.69 ± 0.01	0.00 ± 0.00
L5	~200×400	24.89 ± 0.14	0.23 ± 0.01	0.00 ± 0.00

4. Conclusions and perspectives

Coupling analytical techniques allowed gaining information about the factors influencing the formation of a Mn-rich patina. A possible mechanism could be that Mn-compounds initially present in the sandstones might be dissolved by water (acid rains or water used to stop the 2003 fire) and transported through the porous network, from rock core towards their surface, to feed Mn-rich patina formation as it is assumed for Fe-rich patinas (Nord and Ericsson, 1993). Therefore, since the Luneville castle sandstones have good transfer properties, the main intrinsic parameter conditioning a patina development would be the quantity of Mn initially available in the stone volume impacted by the water, and the solubility of Mn-bearing phases initially present. Indeed, chemical analyses show that patinated blocks are enriched in Mn as compared non-patinated ones. Moreover, Mn appears to be located in specific zones, but in association to different chemical elements according to the sample considered. Determination of the nature of the Mn-bearing phases is thus needed to better constrain the Mn-rich patina formation mechanism. Getting information on Mn-bearing phases is however technically difficult. Laboratory X-ray Diffraction (XRD) experiments did not permit identifying the Mn-bearing phases due to their low content (0.1 and 0.24 weight % of MnO in patinated blocks L2 and L1, respectively) as compared to the total rock. µ-XRD and X-ray absorption spectroscopy at the synchrotron SOLEIL facility (Saint-Aubin, France) on Mn-rich areas will be conducted

in order to help identifying the minerals by coupling structural information with Mn oxidation states.

Acknowledgments

We thank the FLB Company for their financial support and their interest, with a special thanks to Recep Yildirim. We also thank the AGLAE team, especially Quentin Lemasson, for the PIXE analyses, and Mikaël Guiavarc'h for his help with the sample preparations.

References

Beyer, D., 1983, Evolution of reservoir properties in the Lower Triassic aquifer sandstones of the Thuringian Syncline in Central Germany, Dissertation, Friedrich Schiller University Jena, Germany.

Carignan, J., Hild, P., Mevelle, G., Morel, J., Yeghicheyan, D., 2001, Routine analyses of trace elements in geological samples using flow injection and low pressure on-line liquid chromatography coupled to ICP-MS: a study of geochemical reference materials BR, DR-N, UB-N, AN-G and GH, Geostandard Newsletter, 25, 187-198.

Colas, E., 2011, Impact de l'humidité et des solutions salines sur le comportement de grès du Buntsandstein: contribution à la sélection de faciès de restauration, Ph.D. thesis, Reims Champagne-Ardenne University, France.

Géraud,Y., 2000, Perméabilité des roches et loi de Darcy, Planet Terre ENS Lyon, http://planet-terre.ens-lyon.fr/article/permeabilite-des-roches.xml.

Gueguen, Y., Palciaukas, V., 1992, Introduction à la physique des roches, éd. Hermann, ISBN 2-7056-6138-0, 296.

Manceau, A., Schlegel, M. L., Musso, M., Sole, V. A., Gauthier, C., Petit, P. E., Trolard, F., 2000, Crystal chemistry of trace elements in natural and synthetic goethite, Geochimica et Cosmochimica Acta, 64, 3643-3661.

Mertz, J-D., 2010, Etat des lieux, diagnostic des pathologies et perspectives, in: Un chantier, restauration des façades des monuments urbains, Ministère de la Culture et de la Communication, OPPIC, ISBN 978-2-915755-27-5, 8-13.

Nord, A. G., Ericsson, T., 1993, Chemical analysis of thin black layers on building stone, Studies in conservation, 38, 25-35.

Perriaux, J., 1961, Contribution à la géologie des Vosges gréseuses, Mémoires du service de la carte géologique d'Alsace et de Lorraine N°18, Strasbourg University, 236.

Pichon, L., Moignard, B., Lemasson, Q., Pachero, C., Walter, P., 2014, Development of a multi-detector and a systematic imaging system on the AGLAE external beam, Nuclear Instruments and Methods in Physics Research B, 318, 27-31.

Soyk, D., 2015, Diagenesis and reservoir quality of the Lower and Middle Buntsandstein(Lower Triassic), SW Germany, Dissertation, Heidelberg University, Germany.

Thomachot, C., Jeannette, D., 2004, Effects of iron black varnish on petrophysical properties of building sandstone, Environmental Geology, 47, 199-131.